High Throughput, Low Toxic Processing of Very Thin, High Efficiency CIGSS Solar Cells

NREL contract no. XXL-5-44205-08, UCF/FSEC Account no. 2012 8098

Year 3, Quarter 1 Report

Report no. FSEC-CR-1730-07

October 12, 2007

Prepared for

National Renewable Energy Laboratory
1617 Cole Boulevard
Golden, CO 80401

Submitted by

Neelkanth G. Dhere
Florida Solar Energy Center®
1679 Clearlake Road
Cocoa, FL 32922-5703

TABLE OF CONTENTS

1. INTRODUCTION 3

2. OPTIMIZATION OF METALLIC PRECURSOR DEPOSITION AND SELENIZATION/ SULFURIZATION IN THE CONVENTIONAL FURNACE FOR CIGSeS PREPARATION ... 4

3. RAPID THERMAL PROCESSING 7

4. CIGS2 THIN FILM SOLAR CELLS 13

5. $Zn_xCd_{1-x}S$ AS HETEROJUNCTION PARTNER FOR CIGS2 SOLAR CELLS 17

6. REFERENCES 31

1. INTRODUCTION

During this quarter experiments were carried out to use Dimethyl Selenide (DMSe) as a selenium precursor. CIGSeS thin film solar cells prepared by rapid thermal processing were analyzed at Colorado State University and the results are included. Experiments were carried to optimize the CIGS2 solar cell for 1.8 μm thick absorber layer, and encouraging efficiency results have been obtained. Results obtained with alternate buffer layer CdZnS are included.

2. OPTIMIZATION OF METALLIC PRECURSOR DEPOSITION AND SELENIZATION/SULFURIZATION IN THE CONVENTIONAL FURNACE FOR CIGSeS PREPARATION

Highly efficient CIGSeS thin film solar cells are prepared in a two stage process. Firstly, a molybdenum back-contact layers is deposited on sodalime glass substrates by DC magnetron sputtering. Earlier, a thin silicon oxide layer was employed underneath the molybdenum layer to minimize the uneven out-diffusion of sodium from sodalime glass substrate. Currently silicon nitride diffusion barrier is being deposited by reactive magnetron sputtering to act as a more efficient diffusion barrier for sodium. Since the presence of a small amount of Na during growth of the CIGSe absorber layer is beneficial, an optimum amount of Na is deposited on the Mo back contact layer. This is followed by the deposition of the metallic precursors on Mo-coated glass. Next the metallic precursors are selenized and sulfurized in diethyl selenide (DESe) and H_2S ambient respectively. After achieving the highest efficiency of 13.73%, experiments were carried out to improve the material quality to further increase the efficiency. However, the price of DESe have sky rocketed (10 - 12 times) beginning the first quarter of 2007, since many of the companies that supplied the chemical have completely stopped the production. Therefore, an alternative selenium source, dimethyl selenide (DMSe) is being used. It has already given encouraging results. Moreover, a small set-up is being designed and built in collaboration with the UCF Department of Chemistry for the synthesis of DESe using a published process.

1.1 Experimental Technique

The CuGa-In metallic precursors are deposited by DC magnetron sputtering on the Mo coated soda lime glass. The metallic precursors are then selenized in the DMSe ambient. The selenization temperature was in the range of 500 - 550 ºC with varying process parameters, such as dwell at the intermediate and maximum temperature, reactant partial pressures. The process parameters are being optimized to prepare thin film solar cells with device quality material and electrical properties.

1.2 Results and Discussion

Figures 2.1 and 2.2 show the SEM images of the CIGSe thin film solar cells prepared using DMSe as the selenium source. As seen from the images the grains are compact with no porosity. The CIGSe films have shown better adhesion as compared to the earlier films. The J-V measurements were carried out using the in-house setup (Figure 2.3). The device parameters are as follows: V_{oc}: 340 mV, J_{sc}: 25 mA/Cm^2, efficiency: 3.91%.

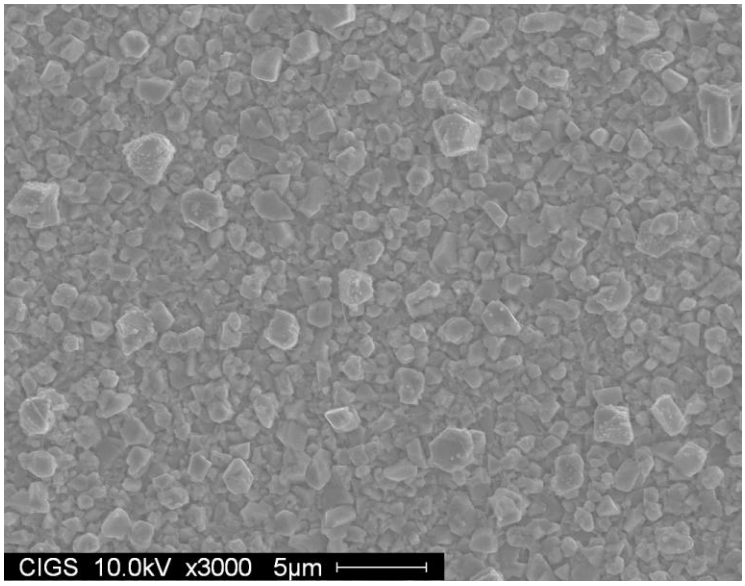

Fig. 2.1: SEM image (x3000) of CIGSe absorber layer prepared at 515 ºC

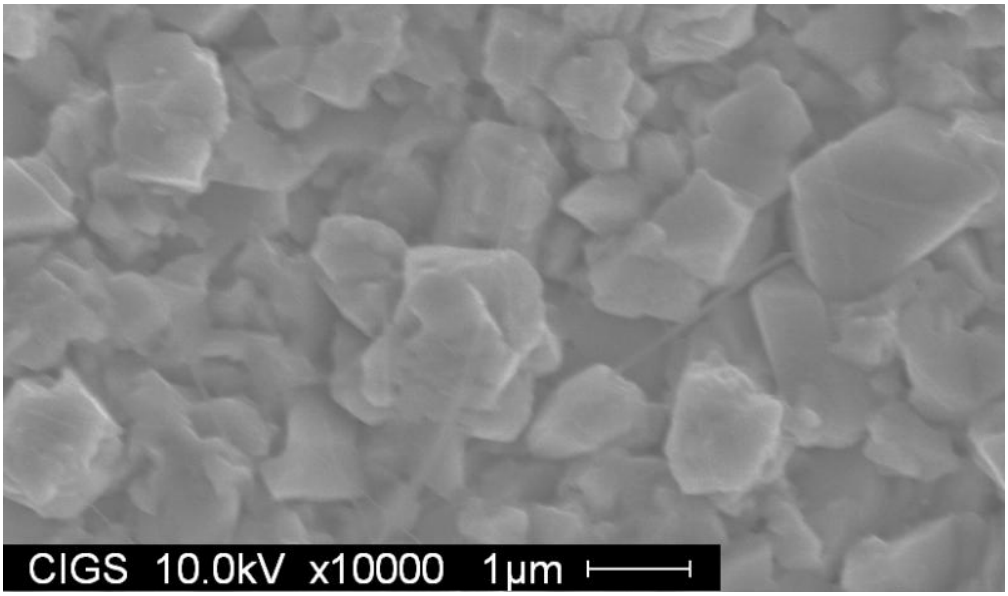

Fig. 2.2: SEM image (x10000) of CIGSe absorber layer prepared at 515 ºC

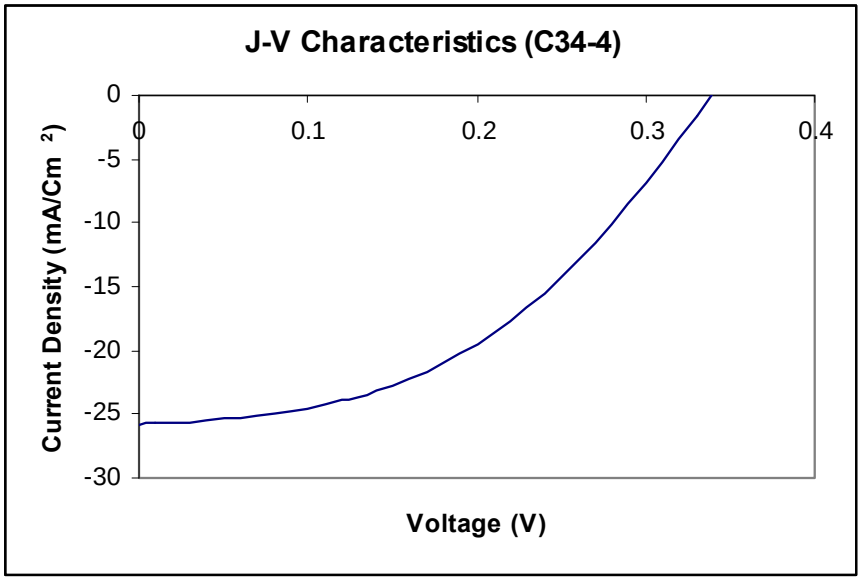

Figure 2.3: J-V Characteristic of CIGSe thin film solar cells prepared using DMSe as selenium source.

Additional experiments are being carried out to prepare CIGSe thin film solar cells with improved device characteristics using DMSe as a selenium source. As described above, a new set up is being designed and built for the preparation of small quantities of the DESe. Successful preparation of DESe will enable the CIGSeS preparation using the two selenium sources viz., DESe and DMSe.

3. RAPID THERMAL PROCESSING

Experiments are being carried out to consistently get higher efficiencies on CIGSeS thin film solar cells prepared by rapid thermal processing. External QE, LBIC and C-V analysis was carried out at Colorado State University (CSU) on the 12.78% efficient cell and the results were provided in year 2 annual report. Further analysis of these cells was carried out by Mr. Galymzhan Koishiyev and Professor Jim Sites at CSU and the results are provided in the following. Figure 3.1 shows the general J-V characteristics. The values obtained are as follows: efficiency 11%, fill factor 58%, J_{sc} = 35.0 mA/cm^2, V_{oc} = 540 mV. The efficiency is reported to be 11% here as against efficiency of 12.78% reported on these cells earlier at NREL. The efficiency reduction is attributed to considerable handling and multiple probing of these cells at various location and transportation from place to place.

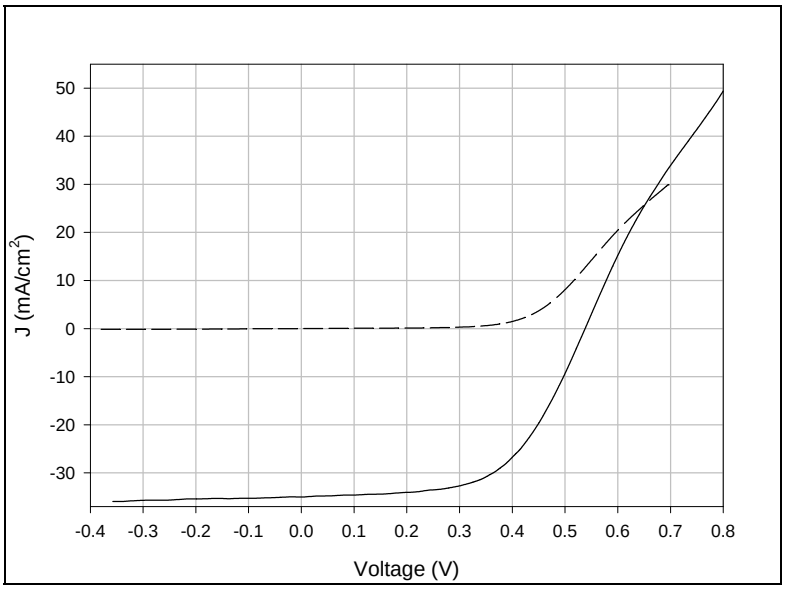

Figure 3.1: Dark and light JV characteristics

Figure 3.2 shows experimental J-V curves at different temperatures from 238 K to 303 K with increments of 5 K. From figure 3.2, one can clearly see the effect of current limitation in forward bias, also known as the rollover effect, which is presumed due to the presence of a back-contact barrier. The rollover effect is very pronounced at low temperatures and disappears as temperature goes higher. The open circuit voltage increases as temperature goes lower and the short circuit current stays almost unchanged on an average at 35.0 mA/cm^2.

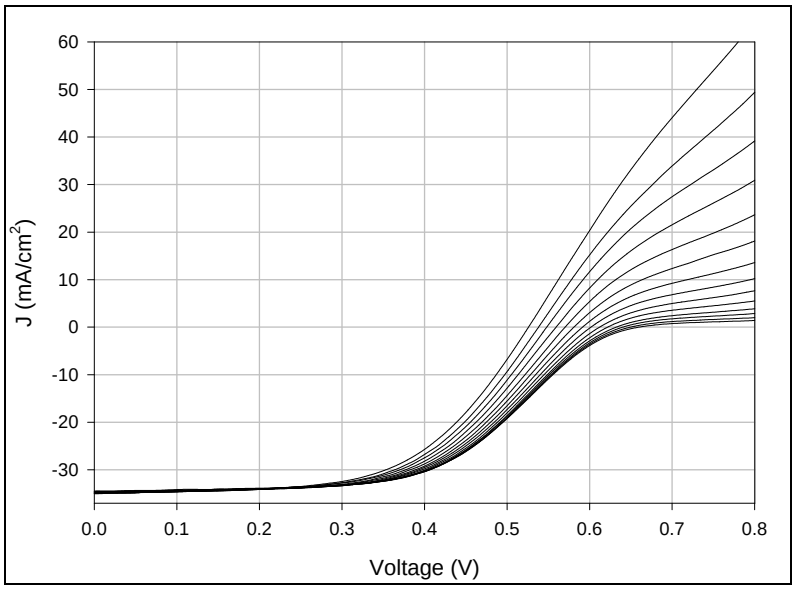

Figure 3.2: Temperature scan

Figure 3.3 shows dependence of the open circuit voltage on temperature. Intercept of the linear extrapolation with the $V_{oc}(T)$ axis gives the band-gap value of the absorber. It is in 1.1-1.2 eV range, as expected for a CIGS device. This result adds credibility to the experimental data.

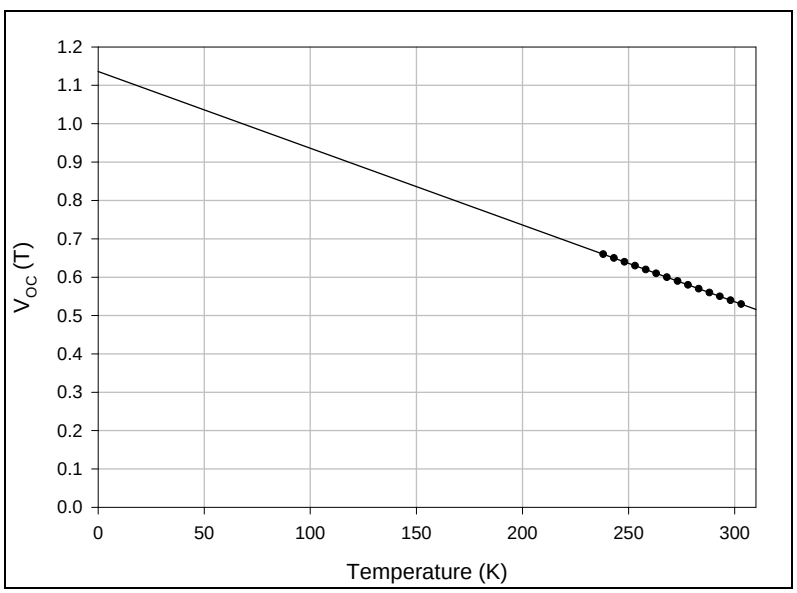

Figure 3.3: Dependence of the open circuit voltage on temperature

Figure 3.4 shows dependence of quantum efficiency and reflection on the wavelength. The quantum efficiency measurement was performed under ~30 mW/cm^2 white-light bias. Integrated product of quantum efficiency and solar spectrum results in 35.0 mA/cm^2 of J_{SC} and matches with the value obtained from J-V measurements, which gives further credibility to the

experimental data. From the part of the quantum efficiency curve between 450 and 550 nm, one can estimate the thickness of the CdS layer to be approximately 50 nm.

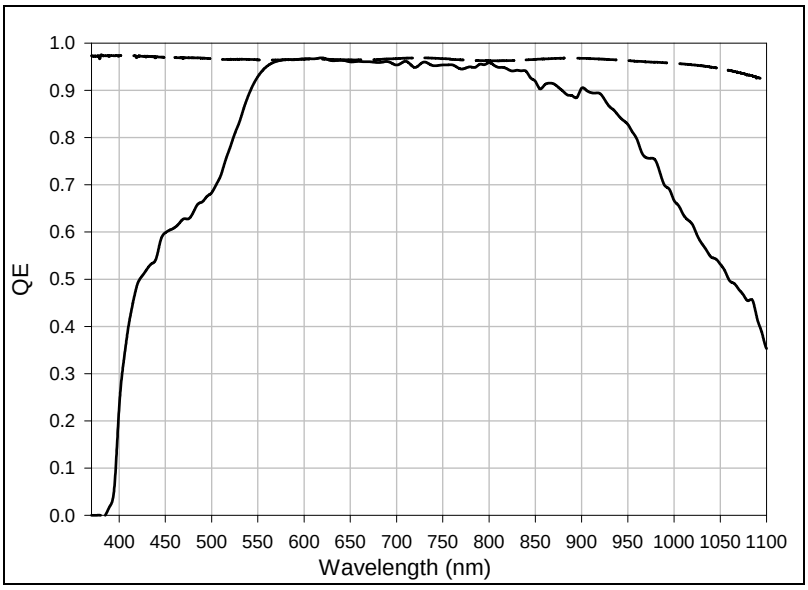

Figure 3.4: Quantum efficiency –solid line, reflection – dashed line

Figure 3.5 shows dependence of the fill factor (FF) on temperature. The fill factor grows steadily from 53 to 58% as temperature increases from about 240 K to 280 K and levels off at about 280K, where the rollover effect starts to disappear. Thus, the rollover effect does not affect fill factor for temperatures higher than 280 K.

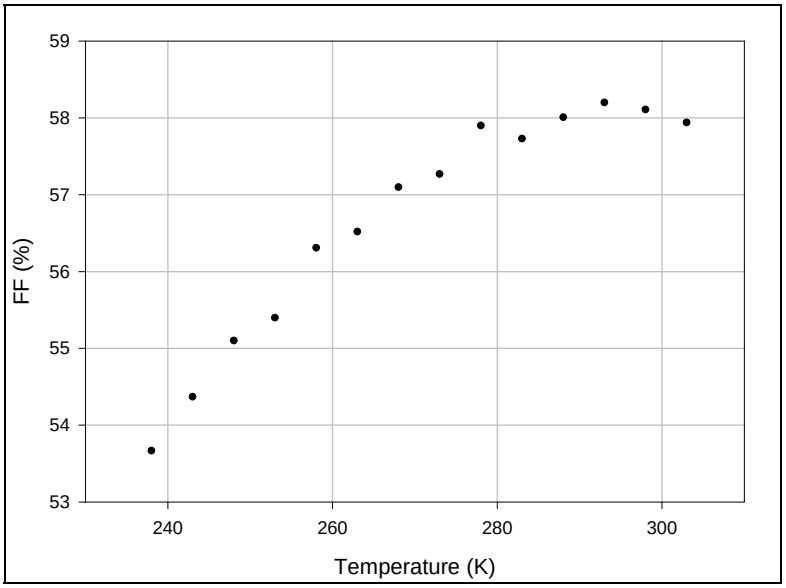

Figure 3.5: Dependence of the fill factor (FF) on temperature

The current at which the effect of rollover takes place, called a turning current, is given by the following expression:

$$J_t = A^* T^2 e^{-\frac{q\Phi_b}{kT}},$$

Where A* is the Richardson constant, Φ_b is the back contact barrier height, T is temperature, k is Boltzman constant and q electronic charge. The back contact barrier height is defined as the difference between the Fermi level in the bulk of the absorber and the valence band at the metal-semiconductor interface.

To find the turning current, one has to take a J-V curve and make two linear fits to the data points just before the rollover and right after the rollover. The intersection of these two straight lines gives a turning point and the current at that point is the turning current. Solid lines in the fig. 6 represent calculated curves of the turning current at different values of the back contact barrier height ranging from 0.40 eV to 0.50 eV with increments of 0.02 eV, and dots are experimental data points found from J-V curves at different temperatures. Figure 3.6 clearly illustrates that the back contact barrier height for the RTP device is about 0.44 eV. The last two points at two highest temperatures show slight deviation from the general trend, because as temperature goes higher, the rollover effect gets weaker and makes it more difficult to find the turning point.

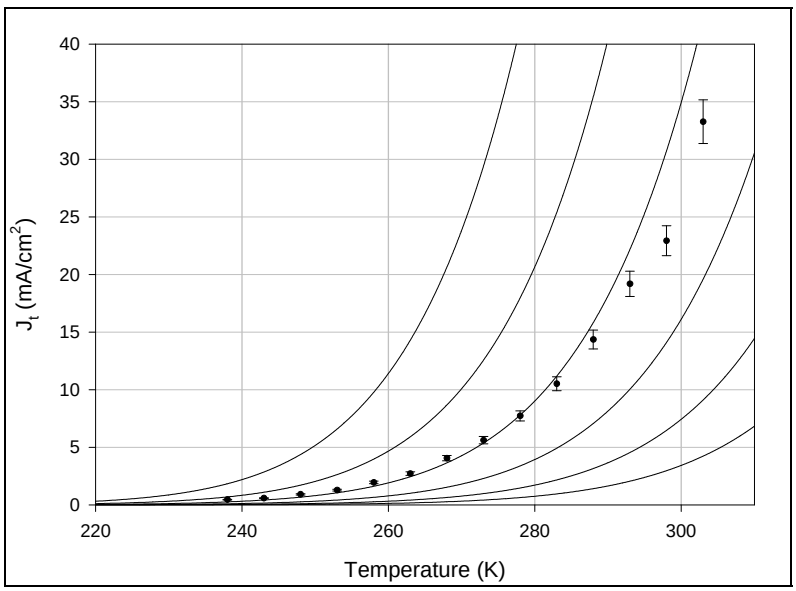

Figure 3.6: Back contact barrier height for cells prepared by RTP

Figure 3.7 is a semi-log version of figure 3.6. From figure 3.7, one can see that experimental data points deviate slightly from the 0.44 eV curve for lower temperatures, as well as for higher temperatures, and agree pretty closely for intermediate temperatures.

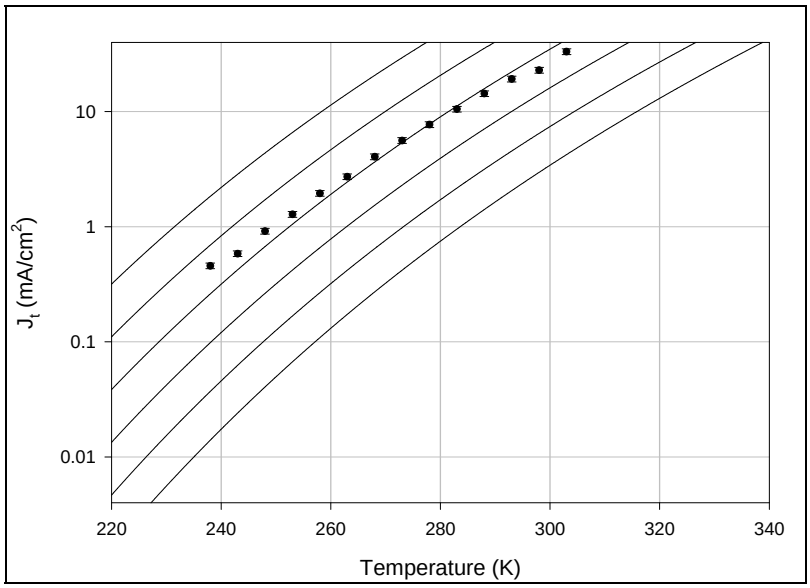

Figure 3.7 Semi logarithmic version of figure 3.6

Figure 3.8 shows C^{-2} dependence on voltage. The data is quite linear on this scale, and the slope gives a carrier density of 4.0×10^{15} cm^{-3}.

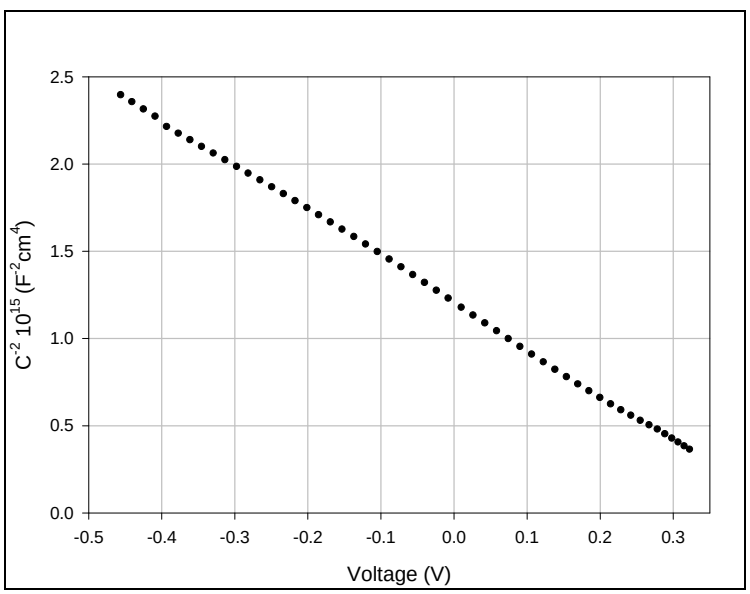

Figure 3.8: Capacitance versus voltage measurement

Figure 3.9 shows Fermi level relative to the valence band as a function of distance from the p-n junction obtained from capacitance-voltage measurements at room temperature. Figure 3.9 strongly suggests that the Fermi level relative to the valence band in the bulk is about 0.21 eV over a significant distance. The Fermi level gets slightly smaller as it comes closer to the depletion layer.

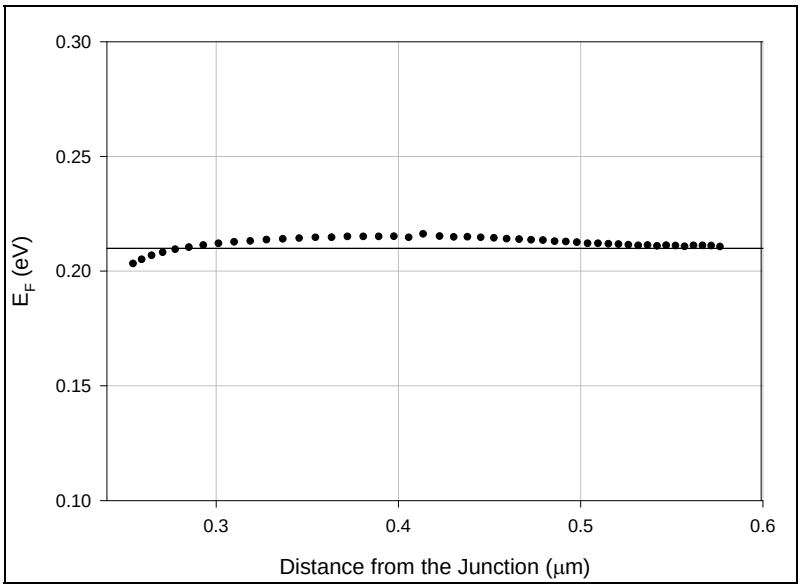

Figure 3.9: Fermi level relative to the valence band as function of distance from the p-n junction

Figure 3.10 is a schematic picture of the band diagram which summarizes all obtained information. A typical value of 2 mm for the CIGS layer thickness is taken. The thickness of CdS layer is taken to be 50 nm as it was estimated from the QE plot.

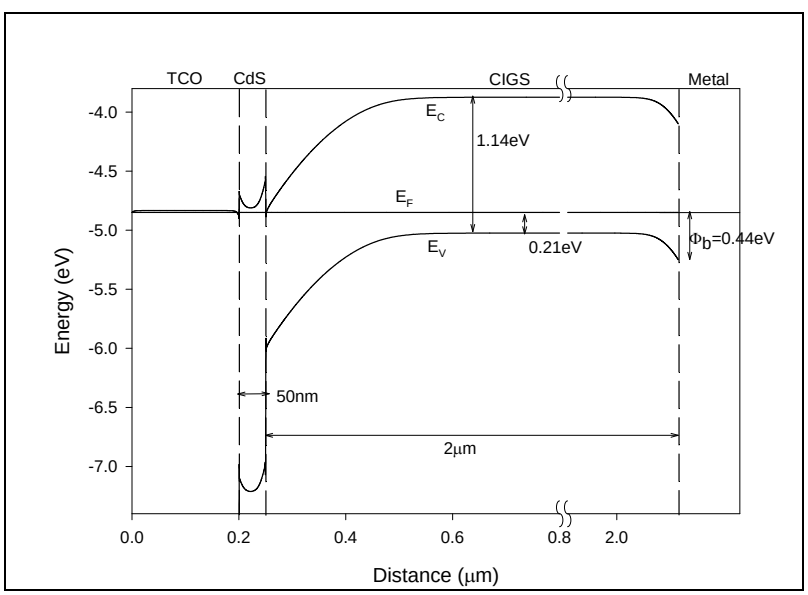

Figure 3.10: CIGSeS thin film solar cell band diagram

This analysis will be useful in designing future experiments for rapid thermal processing of CIGSeS thin film solar cells.

4. CIGS2 THIN FILM SOLAR CELLS

Chalcopyrites are important contenders among thin film solar cells due to direct band gap and higher absorption coefficient. Copper-Indium-Gallium Sulfide (CIGS2) is a chalcopyrite material with a near-optimum band gap of ~1.5 eV. At FSEC PV Materials Laboratory, record efficiency of 11.99 % has been achieved on a 2.7 µm CIGS2 film prepared by sulfurization [1]. Thin-film copper indium sulfide modules are being manufactured by Sulfurcell in Germany. The availability and cost of indium can be a limiting factor for large scale production of CIGS2 thin film solar cells (70 GW_p per year) [2]. The required amounts of metals can be lowered by using a thinner absorber. Efforts are being made to reduce the thickness while maintaining a comparable performance. Initially small size grains are formed during the film growth [3]. With continuing growth to large thicknesses, more favorably oriented grains grow faster and coalesce to form compactly packed large-grain morphology. It is clear that when the thickness of the film decreases, there is possibility of remaining only in the small grain region because the coalescence of grains does not have an opportunity to enhance the grain size to the maximum. Solar cell performance in smaller grain chalcopyrite absorber deteriorates due to larger fraction of grain boundaries [4]. In a series of experiments, CIGS2 solar cell parameters were optimized in the efficiency range of 8-9% for an absorber thickness of 1.8 µm. Of course, the grain size alone does not control the PV parameters. Effective passivation of grain boundaries can reduce the deleterious effects of grain boundaries.

CIGS2 thin films were prepared in two stages. Stage one consisted of the deposition of CuGa-In metallic precursors with Cu/(In+Ga) ratio of 1.4 on molybdenum-coated glass substrates. Stage consisted of sulfurization of these metallic precursors in dilute H_2S (4-8% H_2S) ambient. The copper-rich layer ($Cu_{2-x}S$) that segregated on the surface of near stoichiometric, copper-poor CIGS2 thin film was etched away in a 10% KCN solution. Scanning electron microscopy (SEM) and X-ray diffraction (XRD) were performed at the Materials Characterization Facility at UCF. X-ray diffraction (XRD), I-E and QE analyses were performed routinely at FSEC while selected samples were also analyzed at NREL.

4.1 Scanning Electron Microscopy

Scanning electron micrograph of etched CIGS2 thin film shows (Figure 4.1). It shows well faceted grains.

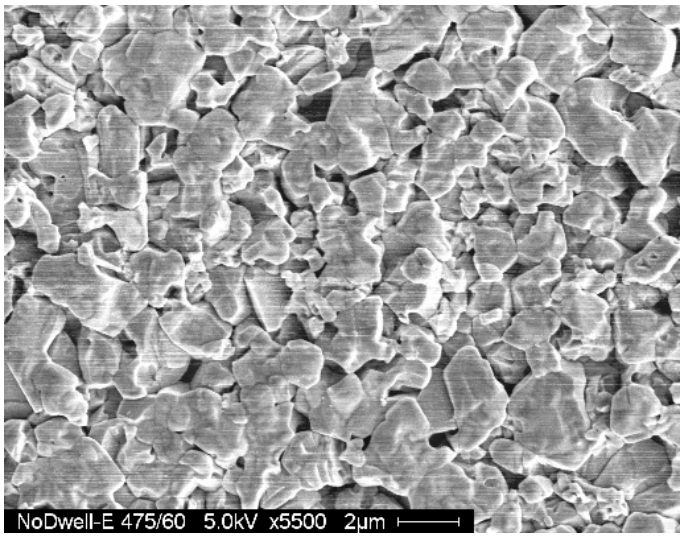

Figure 4.1: Scanning electron micrograph for a 1.8 µm absorber

4.2 X-Ray Diffraction

X-Ray Diffraction (XRD) pattern of etched CIGS2 thin film shows (101), (112), (103), (200), (220), (312) and (400) reflections of highly crystalline chalcopyrite CIGS2 and also reflections from molybdenum (Figure 4.2). The strongest reflection was from (112) plane at 2θ = 27.90°. The lattice parameters calculated were a = 5.51 Å and c = 11.08 Å. Molybdenum reflection was observed at 2θ = 40.6°.

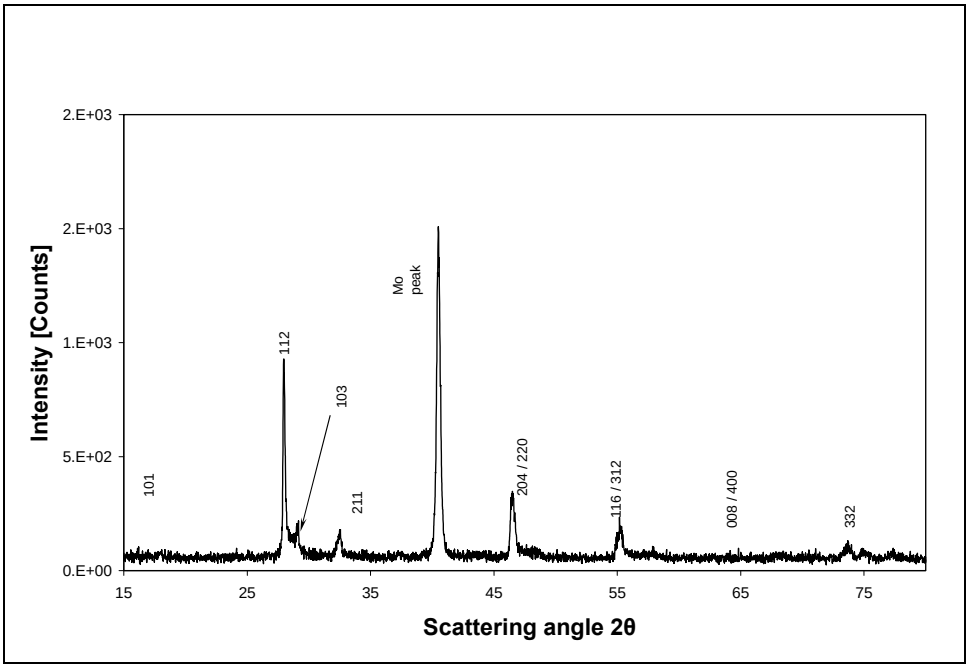

Figure 4.2: XRD for a 1.8 µm absorber

4.3 Photovoltaic characteristics and Quantum efficiency characteristics

Photovoltaic characteristics of CIGS2 thin film solar cells were studied at FSEC and the National Renewable Energy Center (NREL) using current-voltage (I-V) measurement set-up. Figure 4.3 shows the I-V characteristics of CIGS2 solar cell measured at NREL under AM1.5 conditions. Photovoltaic characteristics of the CIGS2 thin film solar cells were as follows: short circuit current density, J_{sc} of 17.52 mA/cm^2, open circuit voltage, V_{oc} of 751.8 mV, fill factor, FF of 66.34% and photovoltaic conversion efficiency, η of 8.74%. Figure 4.4 shows QE characteristics.

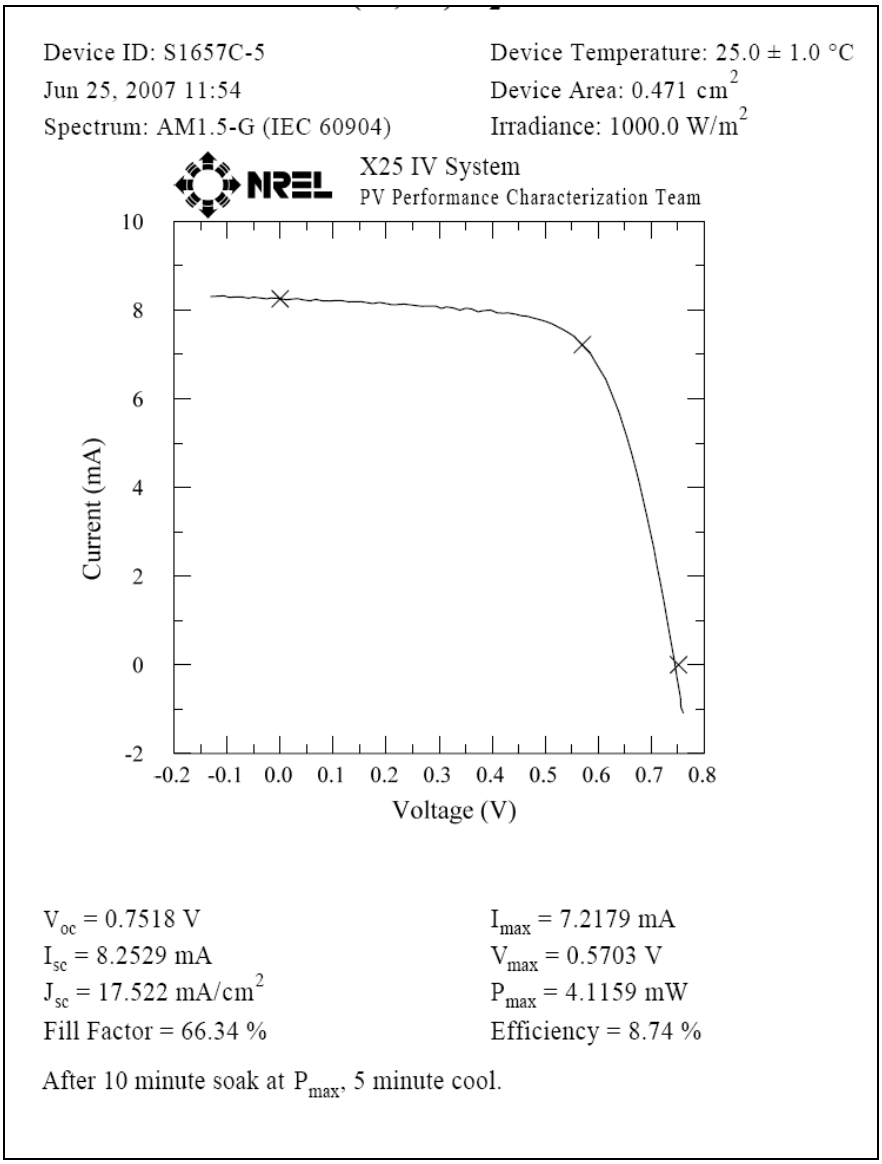

Figure 4.3: I-V characteristics

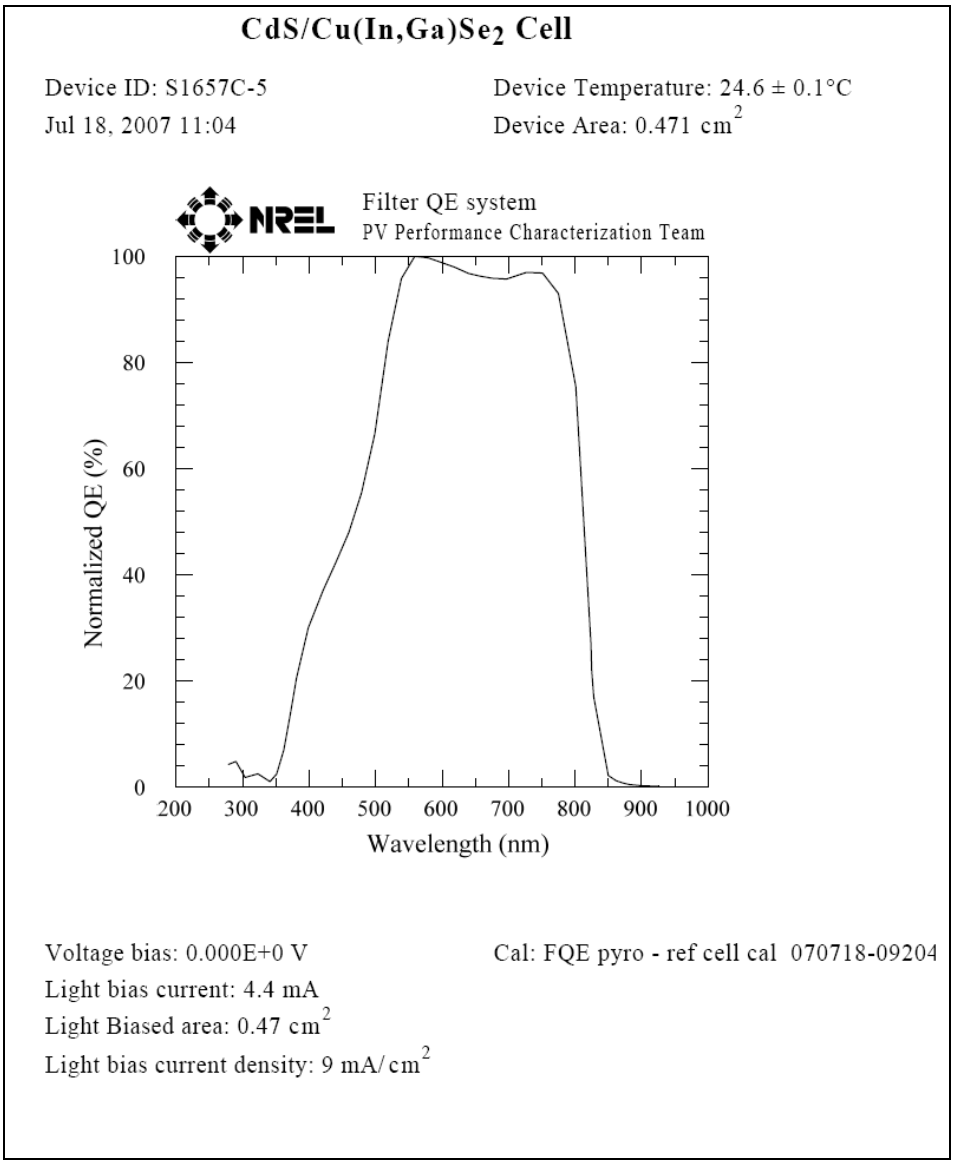

Figure 4.4: Quantum Efficiency characteristics

5. $Zn_xCd_{1-x}S$ AS HETEROJUNCTION PARTNER FOR CIGS2 SOLAR CELLS

CdS heterojunction partner layer has shown high photovoltaic conversion efficiencies with CIGS absorber layer while efficiencies are lower with $CuIn_{1-x}Ga_xS_2$ (CIGS2) absorber layers due to high conduction band offset that result in lower values of open circuit voltage and higher interface recombination [5]. Devices with ZnS heterojunction partner layer have shown better blue photon response due to a higher bandgap as compared to devices with CdS heterojunction partner layer [5, 6]. Moreover, it has been predicted that lower conduction band offset and higher efficiency may be achieved for cells with alternative buffer layer such as $Zn_xCd_{1-x}S$. Therefore, a comparative study, of $Zn_xCd_{1-x}S$ and CdS was carried out to study the probable advantages and applicability of $Zn_xCd_{1-x}S$ as heterojunction partners for CIGS2 devices. Better lattice match of $Zn_xCd_{1-x}S$ with CIGS2 can lead to reduced interfacial recombination resulting in higher voltages. This increase in currents and voltages can result in higher efficiencies as compared to those obtained for CdS/CIGS2 devices.

As described above, CIGS2 absorber layer was prepared by sulfurization of CuGa-In metallic precursors deposited by DC magnetron sputtering. Mo-coated sodalime glass was used as the substrate. An approximately 2-µm thick absorber layer was grown in the copper-rich regime. The substrate was then subjected to etching using dilute KCN solution. The heterojunction partner was then deposited on the CIGS2 absorber using chemical bath deposition. The CIGS2 absorber used for various sets of experiments was not the same. However, for any one set of experiment absorbers from same batch, i.e. fixed Cu/(In+Ga) ratios were used. Moreover, for studying effect of various deposition parameters, a standard composition [6] of reagents was used as reference to study the effect of variation of deposition parameters.

Table I: Standard concentrations used for studying effects of various CBD parameters

	Concentration
$ZnSO_4$	0.02 M
$CdSO_4$	0.2 mM
$(NH_2)_2CS$	0.25 M
NH_4OH	0.58 M

5.1 Influence of ammonium hydroxide concentration

Experiments were carried out to understand the effect of varying NH_4OH concentration and the corresponding pH variation. Various $Zn_xCd_{1-x}S$ films were deposited with 0.09 M, 0.027 M, 0.58 M and 1.2 M NH_4OH. The NH_4OH concentrations were selected so as to maintain the pH of the bath at 9.5, 10.5, 11, and 11.5 respectively. Concentrations of the other chemicals were kept same as the standard solution. Two depositions were carried out at 80 °C for 15 minutes.

Open circuit voltage and short circuit current variation is shown in **Error! Reference source not found.**. Fill factor of 60 and above was obtained at 0.09 M NH_4OH concentration corresponding the bath pH of 9.5 indicating good quality of the film. A high shunt resistance and low series resistance, which are the desired criteria for good quality solar cells, were obtained for film grown at the same NH_4OH concentration. SEM micrographs (**Error! Reference source not found.**, **Error! Reference source not found.**a) show that crystallinity of films grown at pH values corresponding to lower NH_4OH concentrations is higher as compared to that of film deposited with higher NH_4OH concentrations. This explains the higher series resistance at higher NH_4OH concentrations used in chemical depositions due to reduction in crystallinity. Therefore, for high quality solar cells, a very low concentration of NH_4OH and thus corresponding low pH of 9-9.5 is required for chemical bath deposition of $Zn_xCd_{1-x}S$.

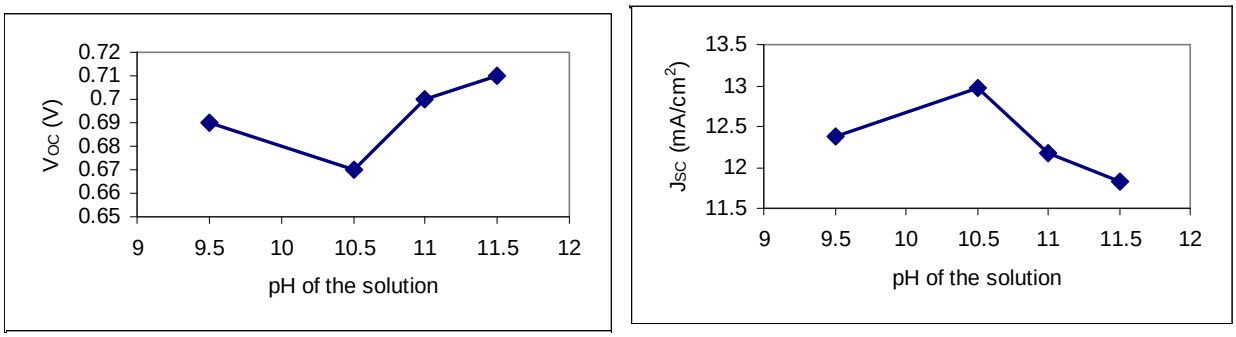

Figure 0.1: Open circuit voltage and short circuit current density values for various pH of bath controlled by NH_4OH concentrations

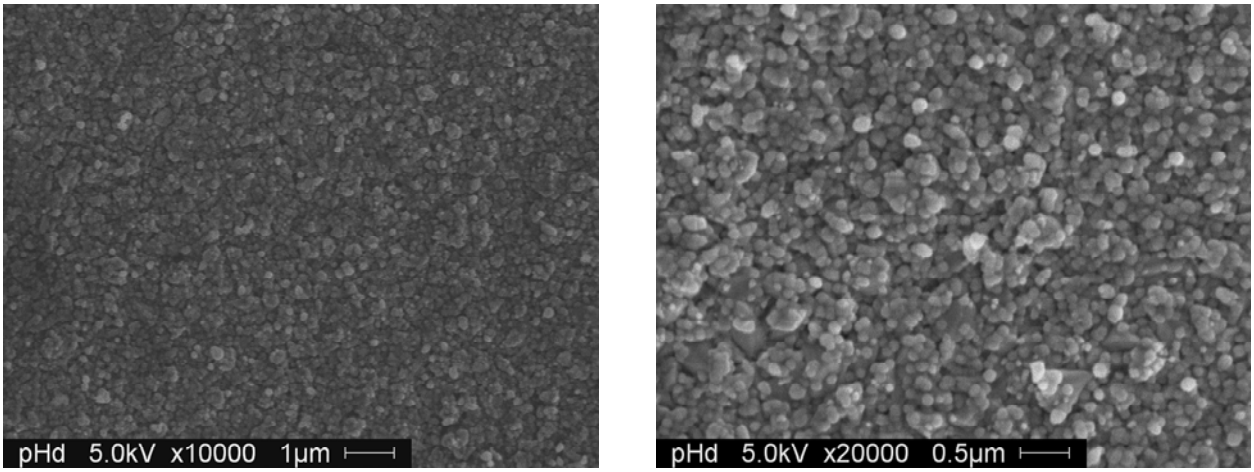

Figure 0.2: SEM micrographs for of the surface of $Zn_xCd_{1-x}S$ film deposited on SnO_2:F glass, with NH_4OH concentration of 0.09 M during chemical deposition.

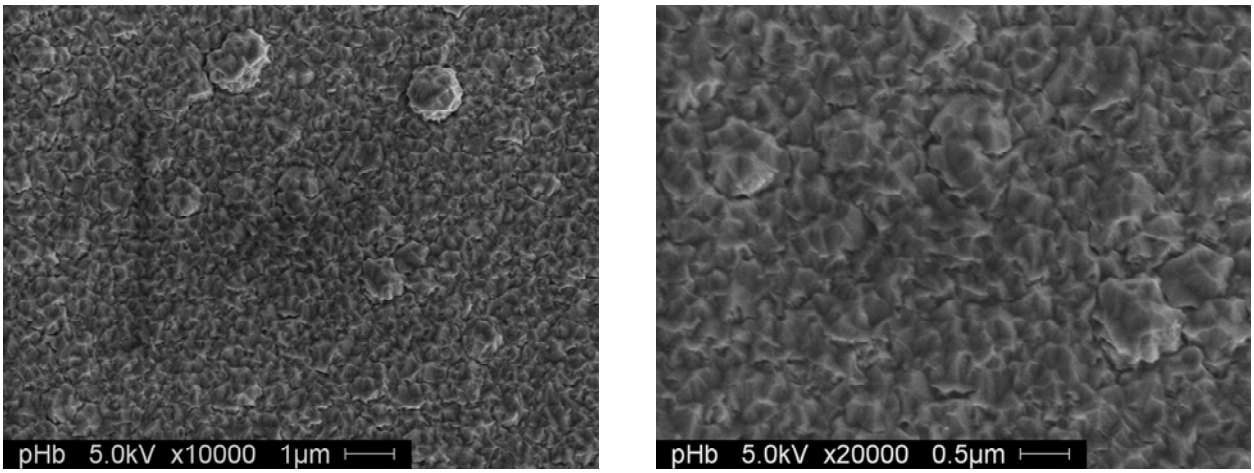

Figure 0.3: SEM micrographs of the surface of $Zn_xCd_{1-x}S$ film deposited on SnO_2:F glass, with NH_4OH concentration of 0.027M during chemical deposition.

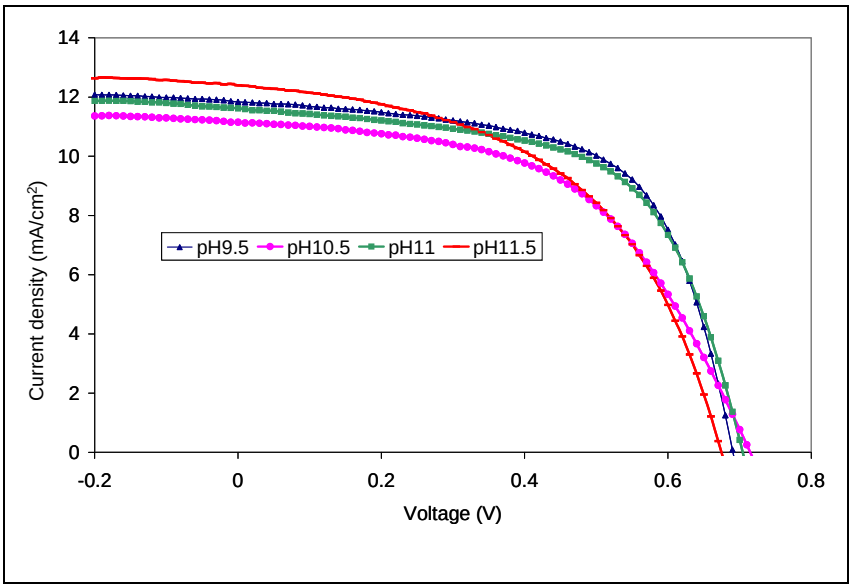

Figure 0.4 The J-V characteristics for CIGS2/ $Zn_xCd_{1-x}S$ prepared at various values of pH of bath adjusted using NH_4OH concentration

5.2 Effect of cadmium sulfate concentration

Concentration of cadmium sulfate, $CdSO_4$ was varied from 0.001 M to 0.003 M keeping the other deposition parameters same as the standard parameters. Increasing concentration of $CdSO_4$ leads to decrease in transmittance of light through the film as shown in **Error! Reference source not found.**. This effect may be attributed to lower bandgap obtained with increasing cadmium concentration in the film. Scanning electron micrographs of films deposited with higher concentrations of $CdSO_4$ during the chemical depositions are shown in **Error! Reference source not found.** and **Error! Reference source not found.**. They reveal better crystallinity and compact grains. Current-Voltage (I-V) characteristics (**Error! Reference source not found.**) indicate that layer deposited with 0.003 M $CdSO_4$ concentration has higher fill factors indicating

good junction properties. As the grains are compact for higher $CdSO_4$ concentration, there are fewer shunt paths leading to improved shunt resistance. Series resistance is lower which indicates that near optimum thickness of $Zn_xCd_{1-x}S$ layer is obtained for this composition. However, the J_{SC} and V_{OC} values obtained for 0.003M $CdSO_4$ concentration were lower as compared to corresponding values obtained for $CdSO_4$ concentration of 0.002 M and 0.004 M. Therefore, fine-tuning of $CdSO_4$ concentration in 0.003M range might result in optimum device properties. I-V curve also indicates that film grown without $CdSO_4$ led to inferior quality cells.

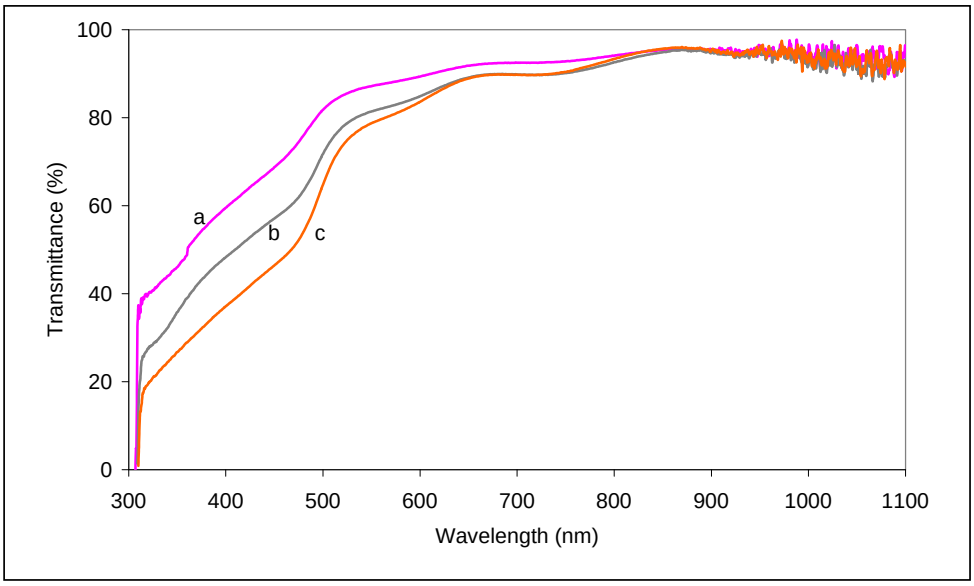

Figure 0.5: Optical transmittance spectra for $Zn_xCd_{1-x}S$ films for varying $CdSO_4$ concentration, (a) 0.001M (b) 0.002M (c) 0004M

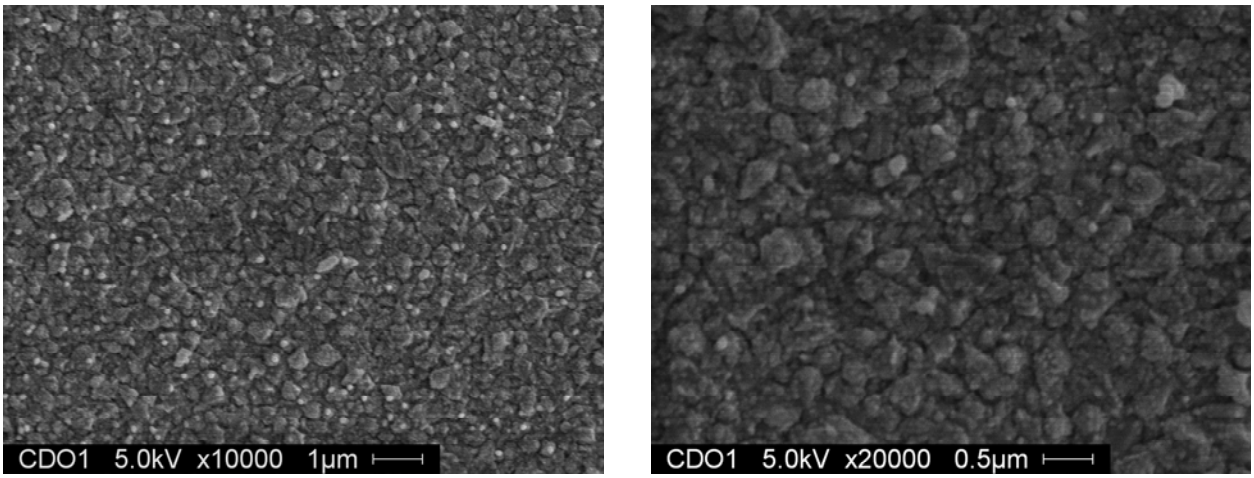

Figure 0.6: SEM micrographs for of the surface of $Zn_xCd_{1-x}S$ film deposited on SnO_2:F glass, for $CdSO_4$concentration of 0.001M during chemical deposition.

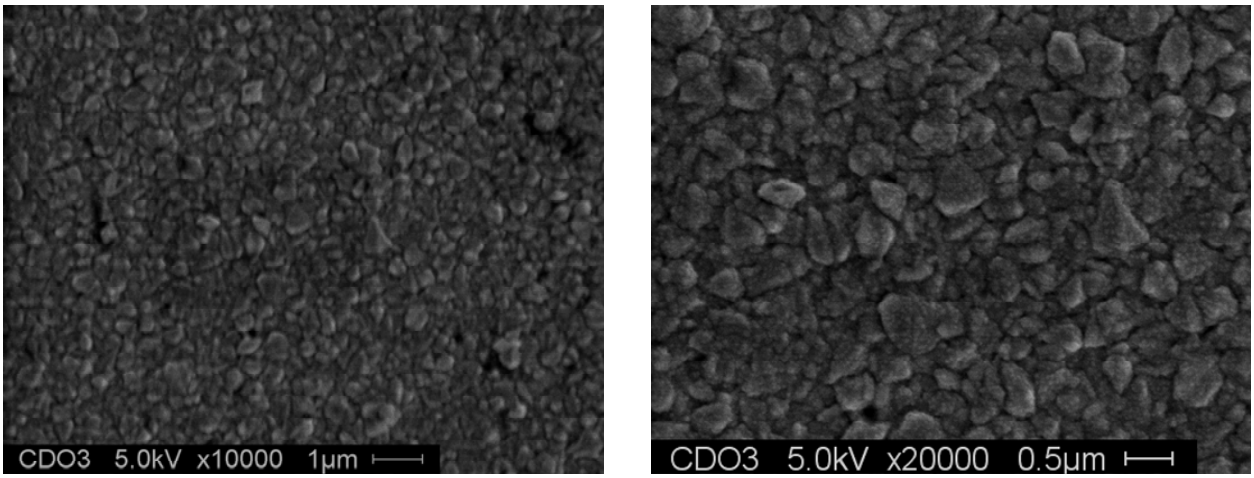

Figure 0.7: SEM micrographs for of the surface of $Zn_xCd_{1-x}S$ film deposited on SnO_2:F glass, for $CdSO_4$ concentration of 0.003M during chemical deposition.

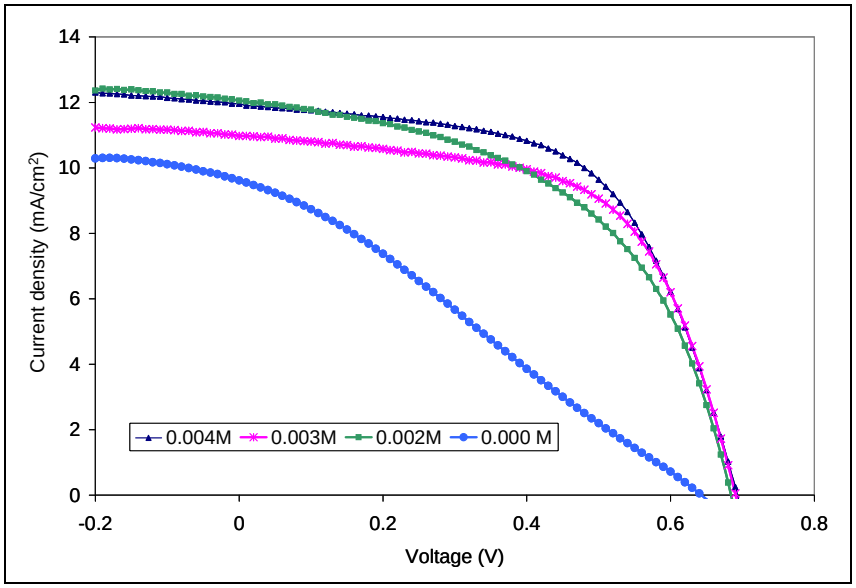

Figure 0.8: The J-V characteristics for CIGS2/ $Zn_xCd_{1-x}S$ device deposited with various $CdSO_4$ concentrations.

5.3 Zinc sulfate concentration variation

The transparency of the heterojunction layer increased with increasing concentration of $ZnSO_4$ in solution in chemical deposition bath as shown in **Error! Reference source not found.**. This effect can be attributed to higher zinc sulfide concentration in deposited films at higher concentrations of $ZnSO_4$ in the chemical bath which leads to bandgap widening thus higher transmittance. SEM micrograph in **Error! Reference source not found.** indicates better crystallinity at higher $ZnSO_4$ concentration in the chemical bath. Higher short circuit current with lower open circuit voltage values were obtained for concentrations of 0.01 M $ZnSO_4$. Slightly lower short circuit current and higher open circuit voltage values are obtained with concentrations of 0.004 M $ZnSO_4$ in chemical deposition (**Error! Reference source not found.**). The reasons

for lower J_{SC} values with increasing Zn content is probably due to unfavorable band alignment between heterojunction partner and absorber layer as the conduction band shifts up with increasing Zinc content in the film. Higher efficiency and better Fill factor values were obtained for concentrations of 0.001 M $ZnSO_4$ in chemical bath. The shunt resistance (~1000 Ω) for all devices with varying $ZnSO_4$ concentration remained almost constant, indicating that the deposition rate is either independent or a very weak function of $ZnSO_4$ concentration during chemical deposition.

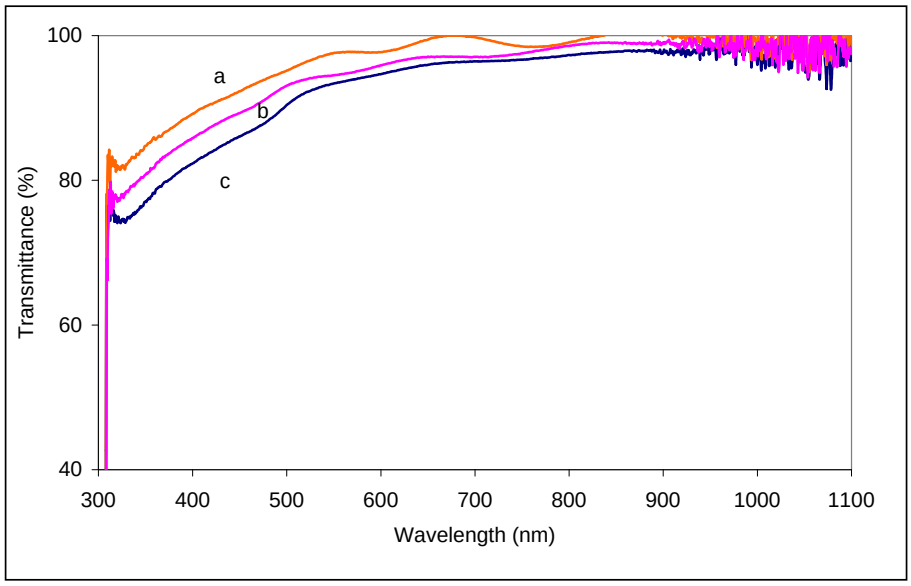

Figure 0.9: Optical transmittance spectra for a single layer deposition of $Zn_xCd_{1-x}S$ films with varying $ZnSO_4$ concentration, (a) 0.04 M (b) 0.02M (c) 0.01 M

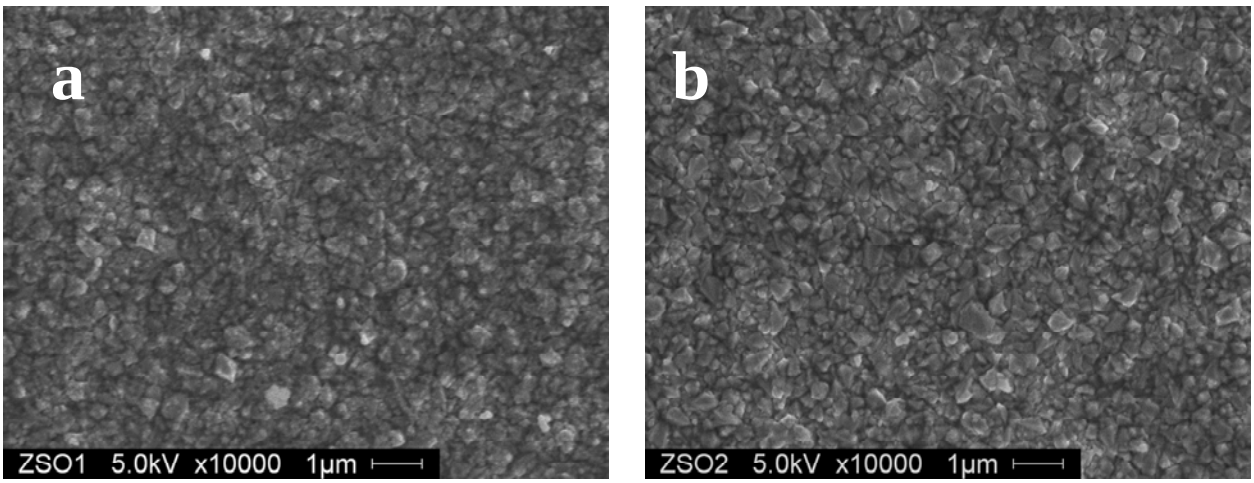

Figure 0.10: SEM micrographs for of the surface of $Zn_xCd_{1-x}S$ film deposited on SnO_2:F glass, for $ZnSO_4$ concentration of (a) 0.01M (b) 0.04M during chemical deposition.

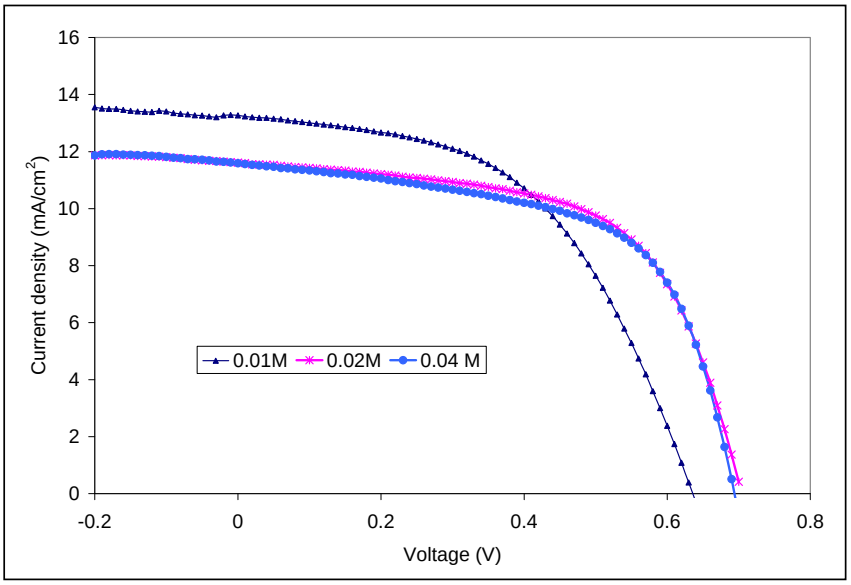

Figure 0.11: The J-V characteristics for CIGS2/$Zn_xCd_{1-x}S$ for various concentration of $ZnSO_4$ in chemical bath.

5.4 Thiourea concentration variation

The transmittance of the heterojunction partner layer increases as the thiourea concentration is increased (**Error! Reference source not found.**). This can be explained on the basis of higher extent of conversion of hydroxides to sulfides in presence of higher concentrations of thiourea since it acts as sulfide source. This results in higher bandgap of deposited film and consequently the higher transmittance. Higher values of open circuit voltage and short circuit current were obtained for lower concentration of thiourea.

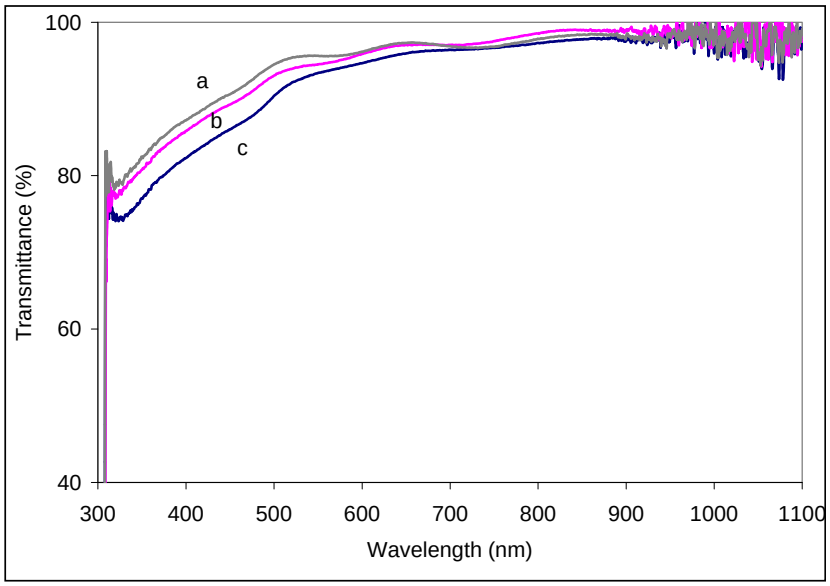

Figure 0.12: Optical transmittance spectra for a single layer deposition of $Zn_xCd_{1-x}S$ films with varying thiourea concentration, (a) 0.375 M (b) 0.25 M (c) 0125 M

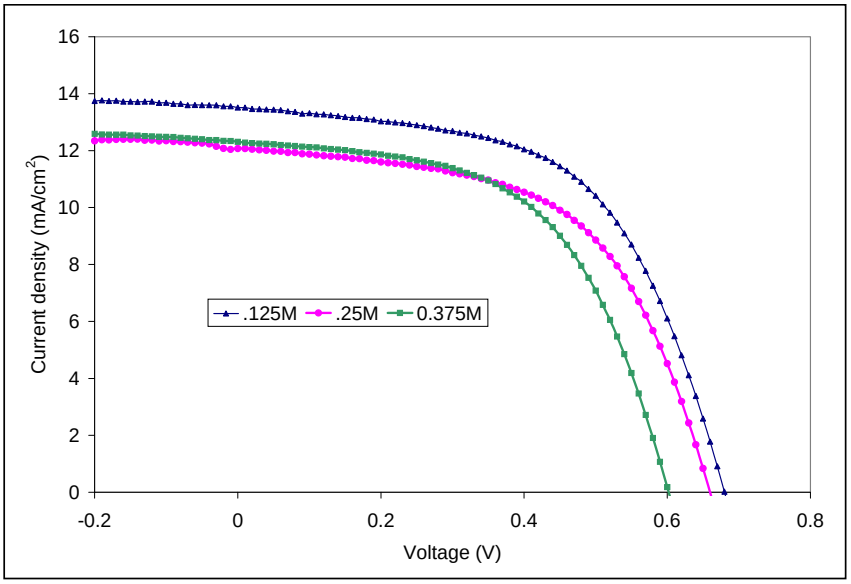

Figure 0.13: The J-V characteristics for as grown and post annealed CIGS2/ $Zn_xCd_{1-x}S$ device.

5.5 Effect of annealing of $Zn_xCd_{1-x}S$ layer after deposition

The samples were prepared by standard deposition parameters. Afterwards, the $Zn_xCd_{1-x}S$ thin film samples were annealed at 200°C for 10 minutes in atmospheric ambient to assist zinc diffusion. The device properties degraded after heat treatment as shown in **Error! Reference source not found.**. This trend is opposite to the trends observed in CIGS solar cells where Zn diffusion helps to improve the device properties. This difference can be explained based on copper-rich CIGS2 growth due to which there is very low concentration of copper vacancies near surface region. Consequently the type inversion does not take place. On the other hand, relatively higher copper vacancies are observed in case of CIGS absorber layer. The vacancies can assists interdiffusion of zinc ions and thus allow zinc to occupy copper site and creation of ZnCu. This helps in the formation of buried homojunctions, hence better device properties.

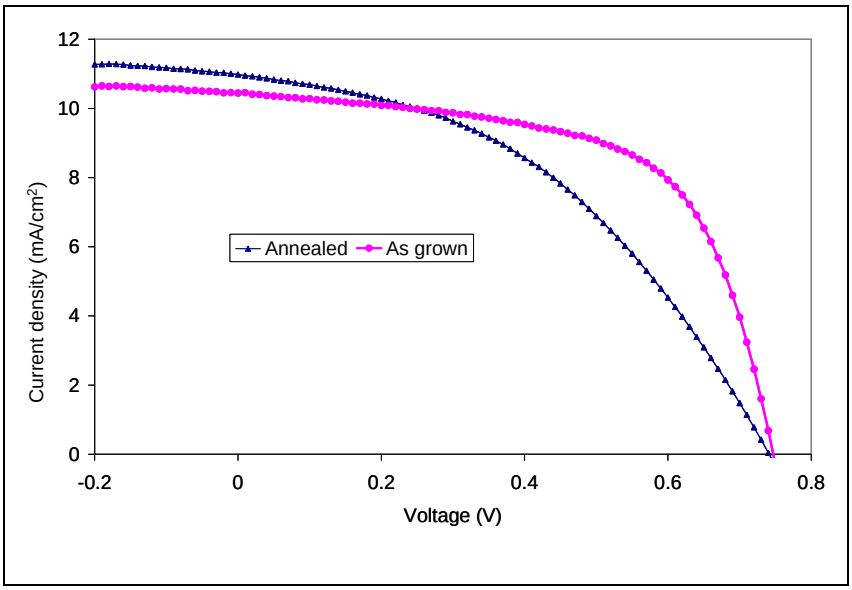

Figure 0.14: The J-V characteristics for as grown and post annealed CIGS2/ $Zn_xCd_{1-x}S$ device.

5.6 Effect of Indium concentration variation in the absorber layer

The lattice parameter of CIGS2 varies between lattice parameter of $CuGaS_2$ (5.35A°) to $CuInS_2$ (5.523A°) depending on In/(In+Ga) ratio. The In/(In+Ga) ratio needs to be optimized to obtain a better lattice match with the heterojunction partner.

The bandgap of the CIGS2 absorber can be increased either by reducing the In atomic concentration or increasing the Ga atomic concentration. With the incorporation of Ga at the near surface region the bandgap increases at the junction and moreover it leads to increase in the conduction band energy. Thus, the spike in conduction band between heterojuction partner and absorber layer, can be minimized by engineering the conduction band position to reach nearer to optimum conduction band alignment condition. The smooth transition from CIGS to CdS due to optimum conduction band alignment allows the minority carriers, i.e. electrons to drift from CIGS to CdS regions without hindrance resulting in better device properties. However, this proposition needs further investigation, as for the CIGS2 absorber prepared by sulfurization; the benefit of Ga alloy is limited since most of the Ga added to precursors ends up the rear part of the absorber near the Mo-back contact.

In this series of experiments, In/(In+Ga) ratio was varied during deposition of metallic precursors by sputtering. To achieve various In content, the thickness of In layer in the metallic precursors was controlled by deposition time. The sputtering system used during the course of this research has a moving substrate mechanism. The thickness of the deposited film is controlled by adjusting the time taken by the substrate to move a unit distance over the sputtering target. Longer duration per unit distance results in thicker layers. Substrate movement durations per inch of 90, 80, 70 and 60 seconds were used. The thickness of Cu-Ga layer was kept constant during this set of experiments. The cell performance for CIGS2/ $Zn_xCd_{1-x}S$ devices improved with decreasing In deposition time. Highest efficiency of 5.45% was achieved for indium deposition duration per inch of 60 seconds. The maximum short circuit current density was obtained for the same device.

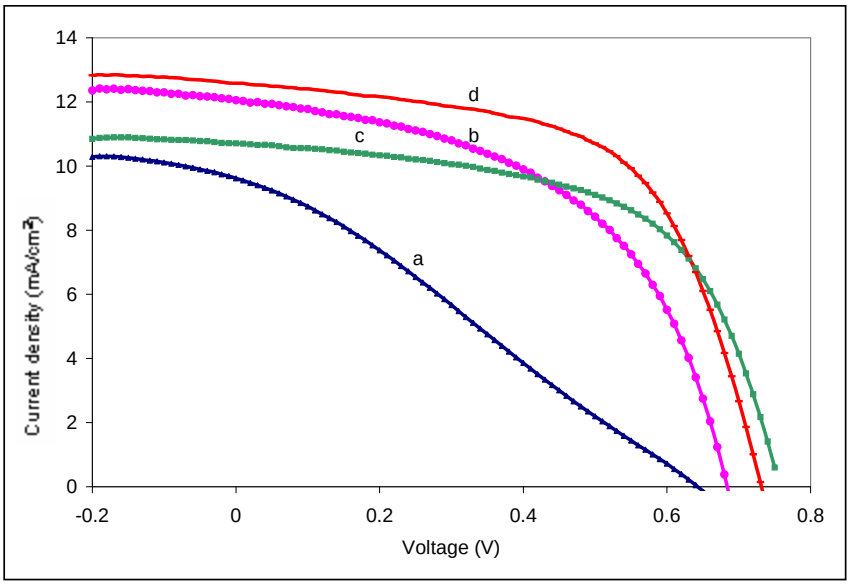

Figure 0.15 The J-V characteristics for CIGS2/ $Zn_xCd_{1-x}S$ device formed with various sputtering time for In metallic precursor deposition for absorber layer formation (a) 90 seconds /inch (b) 80 seconds /inch (c) 70 seconds /inch (d) 60 seconds/inch

5.7 Comparison of CIGS2/ $Zn_xCd_{1-x}S$ and CdS/CIGS2 solar cell

The Current Voltage characteristics (**Error! Reference source not found.** and **Error! Reference source not found.**) measured at NREL shows highest efficiency cell fabricated with $Zn_xCd_{1-x}S$ and CdS as heterojunction partners for 2 µm CIGS2 absorber. The efficiency measured $Zn_xCd_{1-x}S$ as heterojunction partners at NREL was 7.95%, whereas when at FSEC it showed an efficiency of 4.766%. A corresponding increase in efficiencies is expected in all of the results discussed earlier, this is due measurements of lower values of current at FSEC because only a single probe is used. CIGS2/$Zn_xCd_{1-x}S$ has higher open circuit voltage and short circuit current as compared to CIGS2/CdS cell. Whereas for fill factor CIGS2/ $Zn_xCd_{1-x}S$ cell was lower than the CIGS2/CdS. This can be attributed to the highly resistive ZnS film as compared to CdS. To obtain better fill factor $Zn_xCd_{1-x}S$ layer can be suitably doped such that the conductivity of film is enhanced. Current-voltage parameters for both devices are listed in **Error! Reference source not found.**. Cells with $Zn_xCd_{1-x}S$ as heterojunction partners demonstrated even higher efficiencies of 5.45% measured at FSEC.

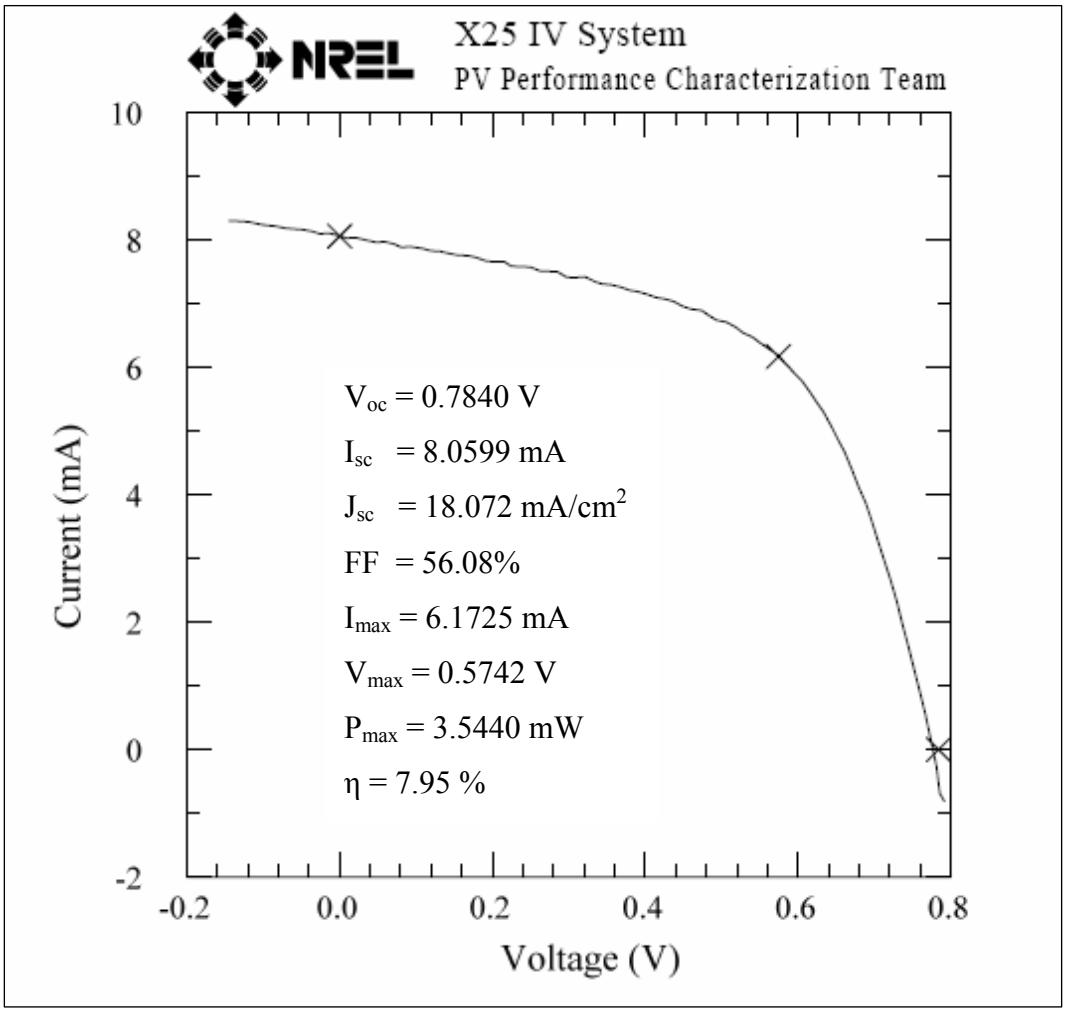

Figure 0.16: The I-V characteristics for SLG/Mo/CIGS2/$Zn_xCd_{1-x}S$/i-ZnO/ZnO:Al devices measured at NREL After 10 minute soak at $P_{max,}$ 5 minute cool.

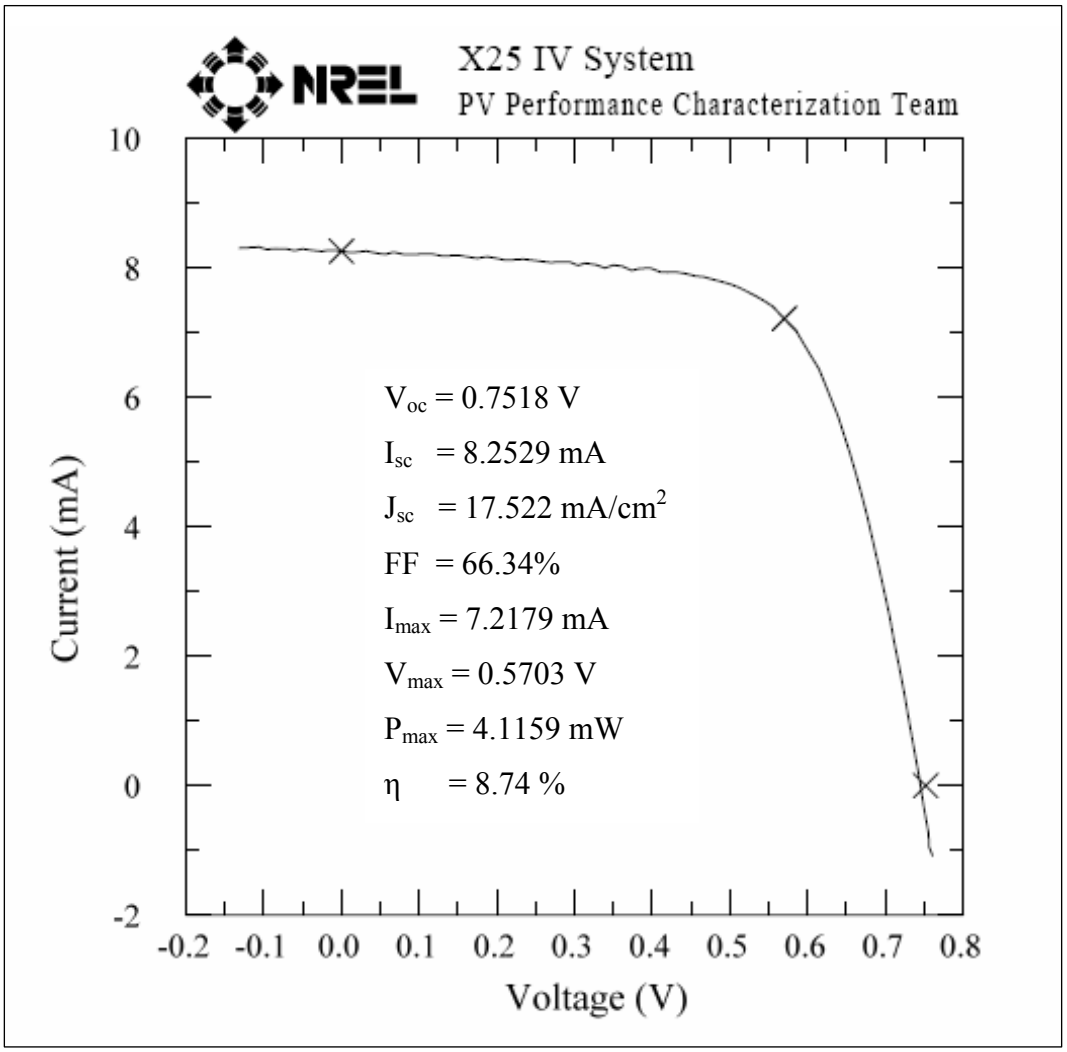

Figure 0.17: The I-V characteristics for SLG/Mo/CIGS2/ CdS / i-ZnO/ZnO:Al devices measured at NREL After 10 minute soak at $P_{max,}$ 5 minute cool.

The quantum efficiency measurement at NREL showed gain in blue photon region for SLG/Mo/CIGS2/ $Zn_xCd_{1-x}S$/i-ZnO/ZnO:Al as compared to SLG/Mo/CIGS2/CdS/i-ZnO/ZnO:Al, **Error! Reference source not found.**, which results in higher J_{SC} values.

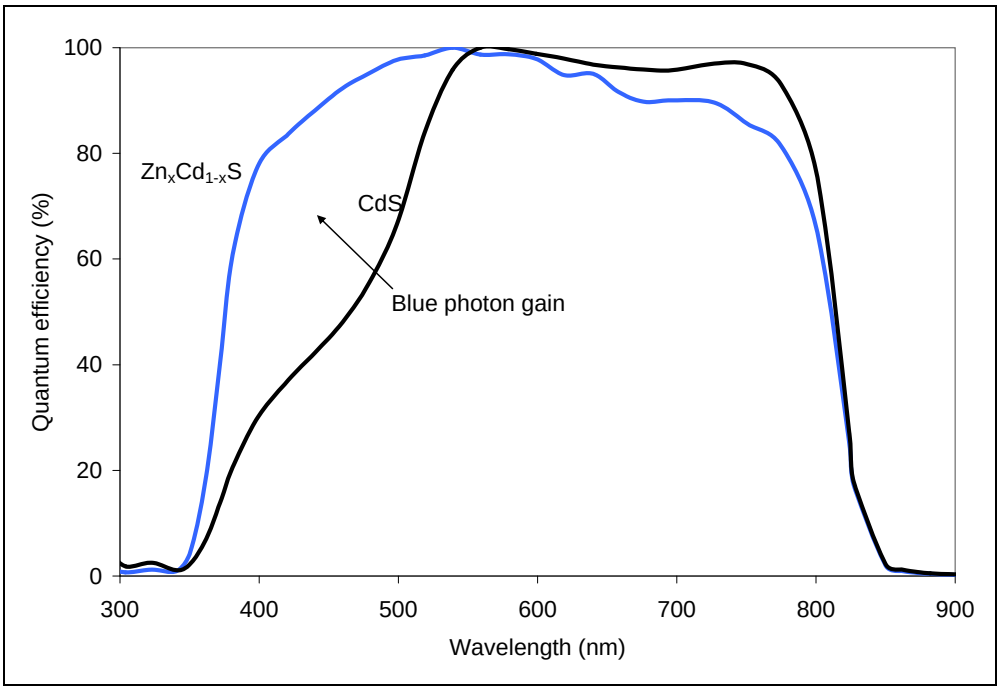

Figure 0.18: Qunatum efficiency plot obtained at NREL for SLG/Mo/CIGS2/CdS/i-ZnO/ZnO:Al and SLG/Mo/CIGS2/ $Zn_xCd_{1-x}S$ / i-ZnO/ZnO:Al cell

The aim of this portion of the work is to recommend and develop an alternative heterojunction partner for CIGS2 solar cells. The study has shown that $Zn_xCd_{1-x}S$ is a strong contender as an alternative heterojunction partner. Effect of various chemical bath deposition parameters on device performance was studied and attempts were made to optimize the deposition parameters in order to improve the device performance. Device properties were studied using current–voltage characteristics. Table 4 summarizes effects of various constituents of CBD on film growth and device parameter. The device performance of CIGS2/ $Zn_xCd_{1-x}S$ solar cells was comparable to CIGS2/CdS solar cells. This indicates that with further optimization of the deposition parameters of the heterojunction partner and improvement in the absorber layer might lead to better device performance of CIGS2/$Zn_xCd_{1-x}S$ solar cells as compared to CIGS2/CdS solar cells. Moreover, it should be noted here that all the efforts towards optimization of the deposition parameters were carried out on ~2µm absorber layer. The crystallinity of the $Zn_xCd_{1-x}S$ layer improved with decreasing pH value of approximately 9.5 of the solution used during the chemical bath deposition. Improved crystallinity resulted in reduction of the series resistance of the devices. Reduction in the In/(In+Ga) ratio in absorber layer resulted in better device parameters, probably due to better lattice matching and/or due to favorable conduction band alignment. The quantum efficiency plot showed blue photon gain, leading to higher short circuit currents. In this study the higher open circuit voltage was obtained for SLG/Mo/CIGS2/ $Zn_xCd_{1-x}S$ / i-ZnO/ZnO:Al as compared to SLG/Mo/CIGS2/ CdS / i-ZnO/ZnO:Al however a lower fill factor was obtained for cells with $Zn_xCd_{1-x}S$ as heterojunction partner.

Table II: Influence of various constituents of CBD on film growth and device parameter

	Parameters				Result summary
	NH_4OH [M]	$CdSO_4$ [mM]	$ZnSO_4$ [M]	$(NH_2)_2CS$ [M]	
A	**0.09-1.2**	**0.2**	**0.02**	**0.25**	**Best at 0.09M eff.=5.07, FF >60% Increasing concentration →decreasing transparency**
B	**0.58**	**0.1-0.4**	**0.02**	**0.25**	**for 0.3mM FF>60% Higher R_p, lower R_s**
C	**0.58**	**0.2**	**0.01-0.04**	**0.25**	**Optimized For~ 0.02M Increasing concentration →Increasing transparency**
D	**0.58**	**0.2**	**0.02**	**0.125-0.375**	**Decreasing concentration.→ higher V_{OC} and J_{SC}**

In this part of study all the parameters are optimized independently. The near optimized parameters need to be clubbed together to optimize the deposition conditions. Further, extensive transmission electron microscopy study to find lattice mismatch, electron and X-ray spectroscopy to study band offsets between absorber layer and heterojunction layer with varying Zn/Cd in heterojunction partner and varying In/(In+Ga) ratio in absorber layer will be required to optimize deposition conditions further.

6. REFERENCES

[1] A. H. Jahagirdar, A. A. Kadam and N.G. Dhere, IEEE 4th World Conference on Photovoltaic Energy Conversion, Hawaii, pp. 557-559, 2006.

[2] B. A. Anderson, C. Azar, J. Holmberg and S. Karlsson, Energy 1998; 23(5): pp.407-411.

[3] J. L. Vossen, and W. Kern., "Thin film processes", New York academic press, 1978.

[4] K. Taretto, U. Rau, J. Werner; Thin Solid Films, 2005:Vol. 480-481, pp. 8-12,.

[5] M. A. Contreras, T. Nakada, M. Hongo, A. O. Pudov, J. R. Sites, ZnS(O,OH)/Cu(In,Ga)Se2 solar cell with 18.6% efficiency. In: 3rd World Conference on Photovoltaic Energy Conversion, Osaka, Japan, May 2003.

[6] R. N. Bhattacharya, K. Ramanathan, L. Gedvilas, B. Keyes Cu(In,Ga)Se_2 thin-film solar cells with ZnS(O,OH), Zn–Cd–S(O,OH), and CdS buffer layers. Journal of Physics and Chemistry of Solids 66(2005) 1862–1864.